DOI: https://doi.org/10.24425/amm.2024.150917

H. ZHANG[1], Z. GUO[2], Z. YUAN[3*]

INDENTATION CHARACTERISTIC STRAIN DETERMINED BASED ON METALLIC MATERIAL DAMAGE

Characteristic strain is a key parameter connecting the hardness and flow stress for indentation experiments. However, there are significant difference between the characteristic strains obtained from previous models. In this work, the indentation characteristic strain is determined based on continuum damage mechanics for Al 5052. Combined indentation tests with the repeated loading--unloading tensile experiments, the indentation characteristic strain is deduced from the reduced Young's modulus. The relationship between indentation characteristic strain and indent depth is established, and the limitation of indentation characteristic strain is determined as 0.12703. From the simulation study, average equivalent plastic strain (PEEQ) is calculated, which also is a function of indent depth. The limitation of average PEEQ is 0.11168, which well agrees with Tekkaya's result (0.112). Furthermore, the relationship between indentation characteristic strain and average PEEQ is deduced.

Keywords: Indentation characteristic strain; Damage; Simulation; Equivalent plastic strain

1. Introduction

It is known that the indentation hardness (H_{Tabor}) is related to the representative stress (σ_r)σ_r as $H_{Tabor} = k\sigma_r(\varepsilon)$, where $\sigma_r(\varepsilon)$ is the corresponding flow stress on the uniaxial stress-strain curve of a certain representative strain, in the range 0.08-0.10 [1]. The representative strain is a key parameter for the indentation hardness, which is also called characteristic strain, effective strain, or average strain [2]. According to Atkins and Tabor [3,4], the representative strains depend only on the cone angle. They revealed that the characteristic strains for metals are 0.3, 0.25, 0.17, 0.11, 0.08 and 0.04 for indenter angles of 30, 45, 60, 68, 75 and 85, respectively. Later, by using expanding cavity model (ECM), Johnson derived the relationship between the representative strain and the indenter angles as $\varepsilon_r = 0.2\cot\theta$ [5]. With numerical analysis method application, Jayaraman et al. [6] suggested that the representative strains are 0.070 and 0.225 for the Berkovich and cube-corner indenters, respectively. Cheng et al. [8] suggested that the representative strain has a function of indenter angles which expressed as $\varepsilon_r = -0.0061\theta + 0.5344$ (for $45° \leq \theta \leq 80°$) through dimensionless analysis.

With the development of computer technology, finite element simulation is increasingly used for studying the indentation experiments, such as the materials stress-strain relationship [7,8], representative strain [9,10] and etc. [11-13]. Dao et al. [9] has proposed a representative strains as 0.033 for inverse problem, which has "no physical basis". Ogasawara et al. took $\varepsilon_r = 0.0115$ for the case of Vickers indentation [10]. Actually, Ogasawara argued that the dimensional analysis used by Dao et al. is questionable because $E/Y > 900$, rather in the range of 25-900 used by Dao et al, for most engineering materials. Therefore, the representative strains depend on not only the indenter angle, but also the material properties and the loading conditions. Representative strain becomes σ_y/E (the ratio between yield stress, σ_r, and Young's modulus, E) independent only when the σ_y/E is with small value [3]. The similar conclusions were found by Bolshakov and Pharr [14].

Furthermore, there are more factors relating to the indentation characteristic strain, such as friction, material dependent [2,15], ratio of loading curvature to reduced modulus. Antunes et al. [15] studied the influence of friction and found that the representative plastic strain is 0.034, which is very near that (0.033) reported by Dao et al. [9]. However, with increasing the material's Young's modulus, it reaches a maximum value, 0.042. Nathan et al. [2] defined the representative plastic strain as the volume average plastic strain within the plastic zone of

1 CNPC TUBULAR GOODS RESEARCH INSTITUTE, XI'AN, SHAANXI 710064, CHINA
2 YIHUANG GAS PROJECT DEPARTMENT OF PETROCHINA CHANGQING OILFIELD COMPANY, YAN'AN, SHAANXI 716200, CHINA
3 CHANG'AN UNIVERSITY, SCHOOL OF MATERIALS SCIENCE AND ENGINEERING, XI'AN, SHAANXI 710061, CHINA

* Corresponding author:yuanyekingfly@163.com

Vickers indentation, which is independent on the amount of prior plastic deformation of the indented material. Through experiments, the predicted indentation hardness is very close to the experimentally measured micro-Vickers indent mapping for the plastic zones of P675 SS and 303 SS. Cao and Huber [16] found that the representative plastic strain is dependent on the ratio of loading curvature to reduced modulus, and they gave the values in the range 0.023-0.095. Chaudhri [17] suggested that the representative plastic strain should be the maximum plastic strain in the plastic zone, which is in the range 0.25-0.36. In fact, there is much higher maximum plastic strains in the indention plastic zone [18,19]. Prasad et al. [20] has studied the influence of indenter angle on the plastic deformation underneath a sharp indenter and on representative strains, and they defined the representative plastic strain as the volume average strain within the elastic-plastic boundary, which is a strong function of indenter angle. They figured out that the universal definition of representative strain determined by $\varepsilon_r = 0.2\cot\theta$ is not valid to determine the values for all conical indentations.

In this study, the indentation characteristic strain under sharp indent is determined based on the damage theory inspired by our previous studies [21-24]. The repeated loading-unloading tests and indention test of 5052 aluminum alloy was coupled to explore the relationship between indention strain and damage. Furthermore, the correlation between the indentation characteristic strain and equivalent plastic strain from finite element method (FEM) was investigated as well.

2. Experimental

The 5052 Aluminum alloy with the chemical composition listed in TABLE 1 was used in this work. Before indentation tests, the specimens were treated by vacuum annealing at a heating temperature of 350°C for 2 hours and cooling to room temperature in the furnace. The samples were ground on 180 #, 400 #, 800 #, 1200 #, and 2000 # sandpaper, respectively. After samples' surface grounding on 2000 # sandpaper, the samples were polished using SiO_2 polishing fluid. Agilent Nano Indenter G200 Tester with a Berkovich diamond indenter was adopted to carry out the Nano-indentation test at room temperature. The tested specimens were separately loaded with maximum indenter loads of 10 mN, 20 mN, 30 mN, 40 mN, 50 mN, 100 mN, 200 mN, 300 mN, 400 mN and 450 mN. The time to load is 15 seconds. Repeated experiments were carried out to obtain data reproducibility which then were analyzed through loading unloading curves. To study the correlation between the strain distribution during indentation, a three-dimensional finite element model was constructed to simulate the indentation process. Finite element method (FEM) was constructed to simulate the indentation process by ABAQUS software (Version 6.14).

TABLE 1

Chemical composition of 5052 Aluminum alloy (wt.%)

Element	Mg	Cu	Mn	Si	Fe	Cr	Ni	Al
Content (wt.%)	2.27	0.14	0.32	0.51	0.31	0.27	0.24	Bal.

3. Results and discussions

3.1. Indentation damage

The *P-h* curves under different loads were depicted as shown in Fig. 1. The loading curves shown similar trend, which indicates a better repeatability of the indentation tests. With the indentation *P-h* curves (Fig. 1), the Young's modulus can be calculated by Oliver-Pharr method [25,26]. The Young's modulus *E* is depicted in Fig. 2. It can be found that the Young's modulus is approximately decreasing with increasing the indentation load (Fig. 2(a)). According to the previous studies, the decreasing Young's modulus was related to indentation damage, which is caused by localized shear stresses during indentation [27-29]. With increasing the indentation load, damage occurs in the material during tests. After unloading, the elastic properties of the tested material decline due to damage accumulation. The unloading curve reflects the damaged material properties with decreased *E*. In Fig. 2(b), the relationship between Young's modulus and indenter displacement is determined from linear fitting. It exhibits good linear relation.

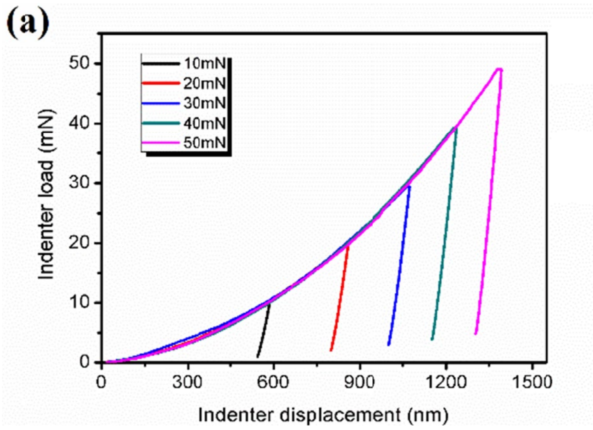

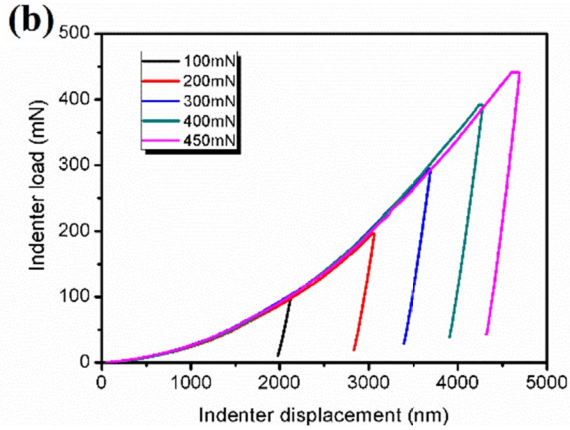

Fig. 1. The *P-h* curves with load range from 100-450 mN in Al 5052

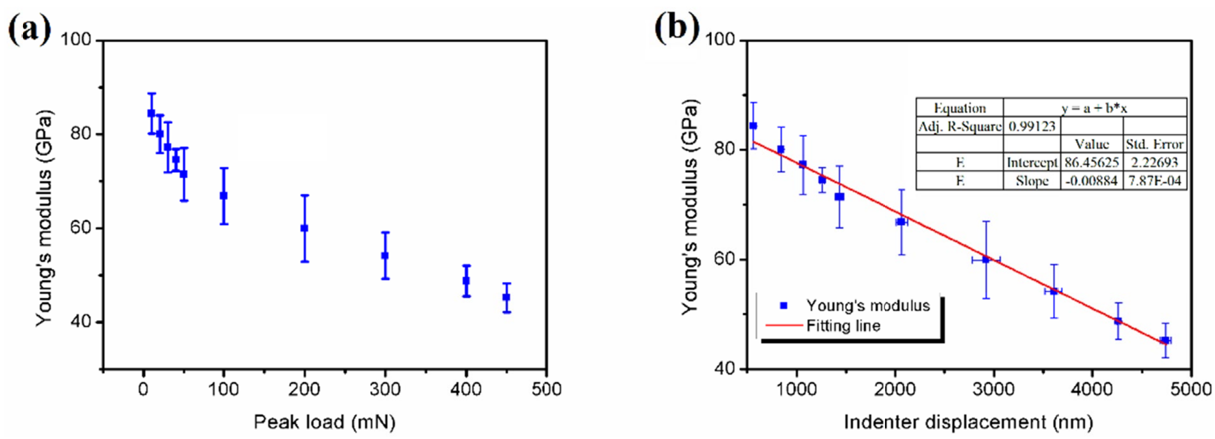

Fig. 2. The Young's modulus of Al 5052 at different (a) peak load; (b) indenter displacement

According to the continuum damage mechanics (CDM), the damage (D_E) for materials is usually determined based on the Young's modulus as [30]:

$$D_E = 1 - \frac{E}{E_0} \tag{1}$$

Where E_0 is the Young's modulus of the material, and E is effective elastic modulus of the damaged material. Accordingly, the indentation damage can be calculated from Young's modulus based on CDM. The results are plotted in Fig. 3, which exhibits significant damage increasing with the indentation load. However, it is noted that the relationship between damage and peak load is not linear. From the view of fracture toughness, the indentation is regarded as a circular crack in the material. According to the fracture toughness equation, $K_{\mathrm{I}} = \sigma\sqrt{\pi a}$, where K_{I} is plain fracture toughness (a material contant). From this equation, there is a relationship between the maximum stress for a material with certain crack length, or the maximum crack length for material under stress. Actually, the maximum stress is contant for a definite material, and it can be considered as the fracture stress. For this, when the indentation depth (crack) increases continuously within the critical depth a_c, the residual bearing depth (a_c-a) is becoming smaller. Meanwhile, the damage increases continuously.

3.2. The indentation characteristic strain determined based on damage

According to the previous work [22] on the repeated loading-unloading tensile carried out on Al 5052, the damage parameter of this alloy was expressed as:

$$D = 1 - \exp(-A\varepsilon) \tag{2}$$

where A = 15.30. One can find that the damage increases with increasing strain.

Assuming equivalent damage for both tensile and indentation, the indentation characteristic strain can be determined from repeated loading-unloading tensile tests. Based on the above indentation damage results, the corresponding strain can be calculated by Eq. (2). Fig. 4 shows the damage and corresponding strain (considered as plastic strain). The damage error bars reflect the damage from repeated indentation test results, and the strain error bars are the corresponding results according

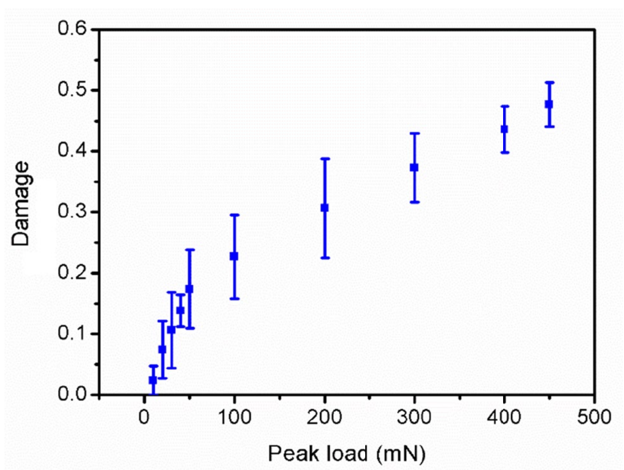

Fig. 3. The Young's modulus damage of Al 5052 under different indentation loads

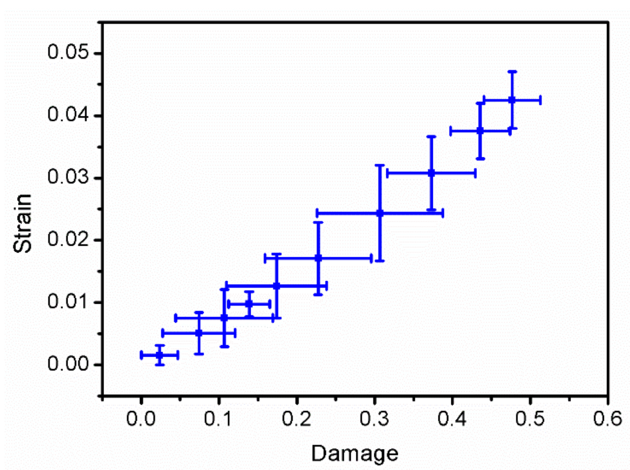

Fig. 4. The damage from indentation experiments versus the corresponding strain from repeated loading-unloading tensile for Al 5052

to damage. It is shown that the strain increases with increasing damage. This reflects the common sense that increasing strain would induce greater damage.

With the determined strain, the indentation displacements with the corresponding strain are plotted in Fig. 5. In addition, the nonlinear fitting was carried out, which shows a good correlation between damage strain and fitting line. The strain can be expressed as a function of indentation depth h (nm) according to the fitting results:

$$\varepsilon = 0.12703 - 0.13192\exp(-9.17\times10^{-5}h) \tag{3}$$

As seen in Fig. 5, the Eq. (3) is a positive function with indenter depth, which increases with increasing the h. When the indentation depth is shallow, the strain is small. While the indent depth is deep, the strain increases. However, the maximum limit of Eq. (3) can be deduced as 0.12703, when h has a very great value. So, when the limit strain obtained can be considered as the characteristic strain at macroscopic scale. Furthermore, it is found that the value of the limit strain is greater than the characteristic strains from Tabor [1] (ε_r = 0.08) and Johnson [31] (ε_r = 0.2cotθ = 0.07), but it is close to Tekkaya's result (ε_r = 0.112 [32]).

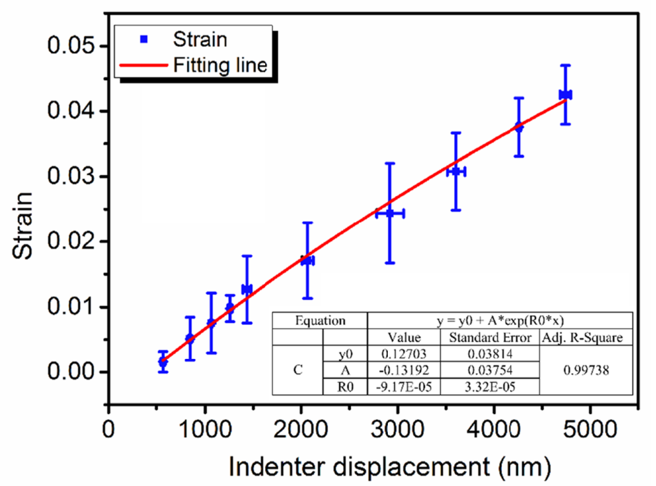

Fig. 5. The strain vs. the corresponding indenter displacement for Al 5052

From the relationship between the strain and the indenter displacement, the relationship between damage and indenter displacement can be rewritten as:

$$\begin{aligned} D_{E,Indentation} &= 1-\exp\left(-A\varepsilon\right) \\ &= 1-\exp\left[-A\begin{pmatrix}0.12703-0.13192\\ \exp\left(-9.17\times10^{-5}h\right)\end{pmatrix}\right] \end{aligned} \tag{4}$$

For further deduction, it can be known that the damage is zero when the indenter displacement is 0 nm. This means that when the indenter permeates the sample, the damage has started. With increasing the indentation displacement, damage further takes place. This implies that there is no threshold value for the damage in 5052Al to begin during indentation experiment with Berkovich indenter, because damage is always accompanied by indentation process.

Based on Eq. (4), the indentation damage can be depicted as Fig. 6. As shown, the indentation damage increases with increasing the indentation displacement. The value of damage is 0.85 when the indentation displacement is at least greater than 40000 nm (40 μm) from Fig. 6. When the damage is 1, the material under indenter should fail according the damage theory. However, the limit of indentation damage is less than 1 with large indentation displacement. It means that Al 5052 would not fail. That is why many ductile materials, such as Al and Cu, hardly show indentation crack. From Eq. (4), the indentation damage at different indenter displacement can be predicted. Fig. 7 shows the comparison between predicted damage from Eq. (4) and damage from Young's modulus $\left(D_E = 1-\dfrac{E}{E_0}\right)$. It can be found that the predicted damage is very close to the Young's modulus damage, and the value of predicted damage is within the error range of Young's modulus damage.

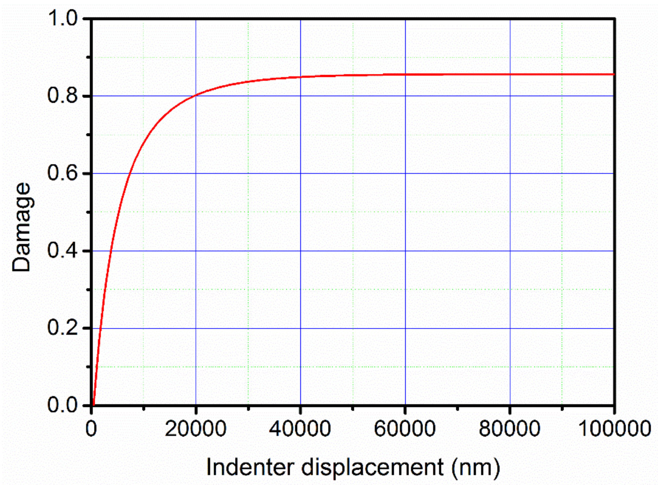

Fig. 6. The indentation damage vs. indentation displacement

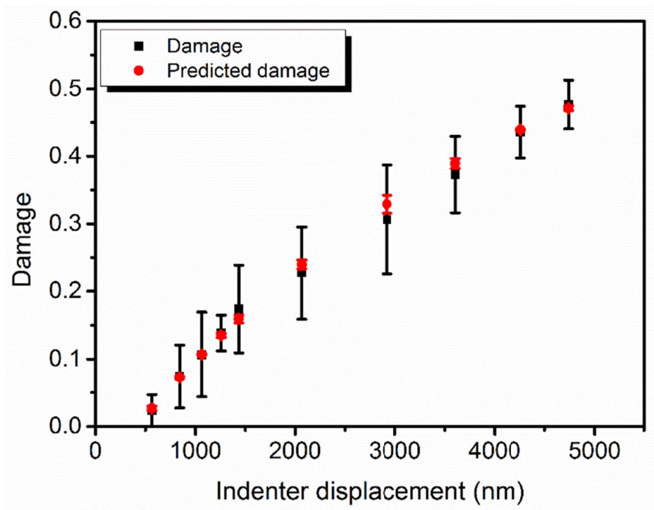

Fig. 7. The damage and predicted damage at different indenter displacements

To some extent, the elastoplastic properties of metals are reflected as the degree of metal interatomic bonding force to resist external forces. The elastic modulus of a material is a macroscopic manifestation of the interaction between atoms. Plastic deformation is the result of internal defect movement, especially for dislocations and twins. Dislocations and twins are the barrier of plastic deformation of most ductile metal materials. When the local stress concentration is equal to or greater than the atomic bonding force after initiation of dislocations or twins and movement reaches the critical state, the microdamage would nucleate under a low external stress. In the process of material deformation, a large number of slip or twin would be produced. Dispositional motion (slip or climb) [33-35], atomic surfaces arranged in regular pairs separate and recombine, which would load to numbers of mismatched micro atoms. With deformation propagates, mismatches would increase and the accumulation of mismatches would lead to microscopic defects, such as holes and micro-cracks. This affects the atomic rebound deformation, thereby declining the resilience from the original regular arrangement of materials and the performance of in elastic modulus. Plastic deformation damage of a material is a process of cumulative evolution across scales [36]. To some extent, there is a positive correlation between the deformation degree of material and the atomic mismatch. With the increase in deformation, the atomic mismatch increases, which leads to a proportional increase in the numbers of holes or cracks and to indirectly degrade the elastic modulus.

3.3. The strain determined from FEM

The size of specimen was Φ100×50 μm. As shown in Fig. 8, the designed model contains 37400 elements using 8-node linear brick elements (C3D8) and the Berkovich indenter part includes 344 elements using discrete rigid (R3D4). During simulation, the frictionless tangential behavior was applied to the contact between indenter and material. In simulation, the adopted plastic stress-strain relation of specimen was adopted from the repeated stress-strain curve. The bottom of the model was fixed during indenter loading. Five displacement loads were given according to the above indentation experiments as 2.07 μm (100 mN), 2.92 μm (200 mN), 3.60 μm (300 mN), 4.26 μm (400 mN) and 4.74 μm(450 mN). Fig. 10 shows the distribution of simulation results for 300 mN. It can be found the shapes of the isoline of equivalent plastic strain (PEEQ) distribution at maximum depth are similar.

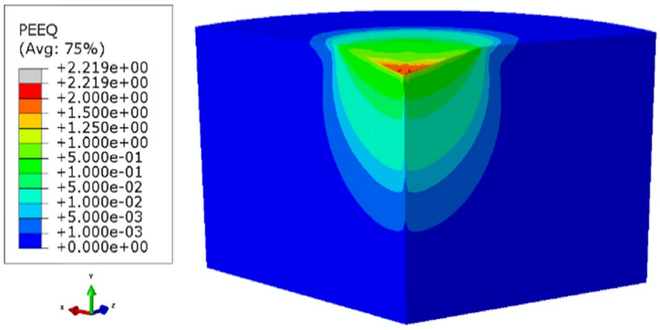

Fig. 9. The PEEQ results of 300 mN at maximum depth

For quantitative analysis of strain distribution in simulation results, a statistical method has been introduced. Based on the simulation results, PEEQ of the model can be obtained using the following algorithm [37]:

$$V_s = \left[\sum_{k}^{N_s} V_k\right], \quad \varepsilon_{ps} = \frac{1}{V_s}\left[\sum_{k}^{N_s} \varepsilon_{pk} V_k\right] \tag{5}$$

In Eq. (5), V_s and ε_{ps} are the total volume and the average PEEQ in the plastic zone, where the PEEQ is greater than 0; V_k and ε_{pk} are the volume and the PEEQ of the k^{th} element, respectively; and N_s is the total element number. The average PEEQ for the selected elements were calculated based on the post-process simulation results via the ABAQUS script language Python. The statistical average PEEQ is shown in Fig. 10 for different maximum loads. With increasing the indentation displacement, the average PEEQ basically increases, and these five

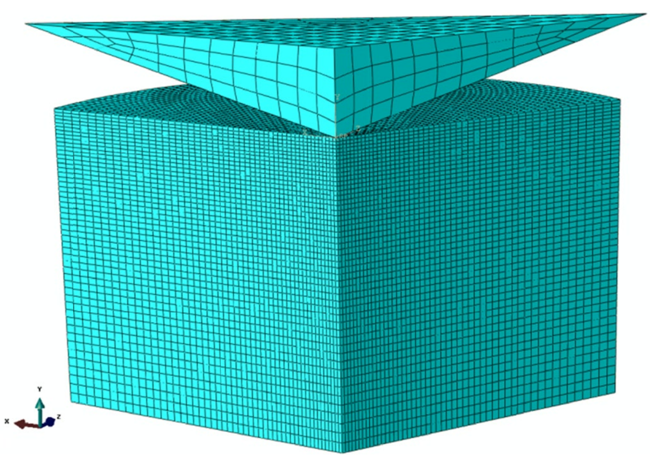

Fig. 8. The designed simulation model

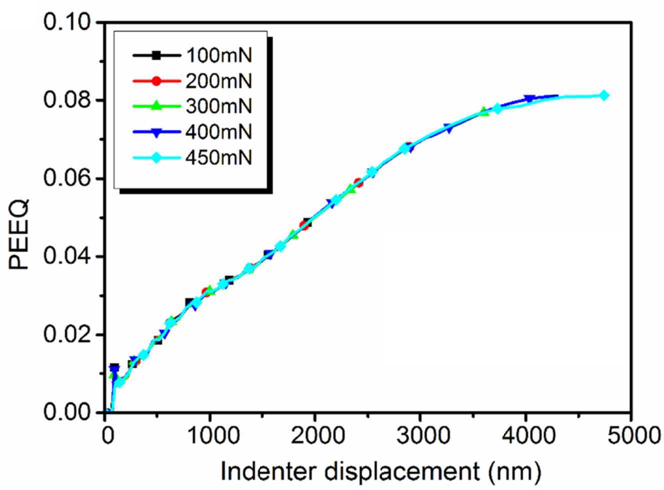

Fig. 10. The average PEEQ with different peak loads

curves are coincided. Actually, the plastic strain region increases linearly with the increase in indentation depth [38], so the curves have the same trajectory for greater loads.

Furthermore, the average PEEQ at different indentation depth were calculated, and the results are shown in Fig. 11. It seen from Fig. 11, with increasing the indentation depth, the results of average PEEQ increase continuously, which are well consistent with the results shown in Fig. 11. In addition, it can be found that this increasing trend presents a nonlinear increase with the increase in indentation depth, and the increasing degree gradually slows down after 4500 nm. The nonlinear relationship between the average PEEQ and the indentation depth can be regressed using an exponential function. The equation can be expressed as:

$$PEEQ_{FEM}(h) = \\ = 0.11168 - 0.10939\exp(-3.00083\times10^{-4}h) \qquad (6)$$

As per Eq. (6), the average PEEQ is a function of indenter displacement, which is increasing with increased indentation depth. Furthermore, one can find from Fig. 10 that the minimum limit of average PEEQ is 0, when the indentation depth is 0. As the indenter penetrates into the material, the PEEQ begins to produce. Also, it can be found that the maximum limit of average PEEQ is 0.11168 when the indentation depth is much great, which is much close to Tekkaya's result $\varepsilon_r = 0.112$ [32]. The average PEEQ and Tekkaya's result are identical, even though they are obtained from different simulation methods. The maximum limit of average PEEQ is the result for much great indentation depth. The great indentation depth can be considered as the macro indentation, where most materials show a depth independent hardness with the indentation depth greater than 10 μm [39,40].

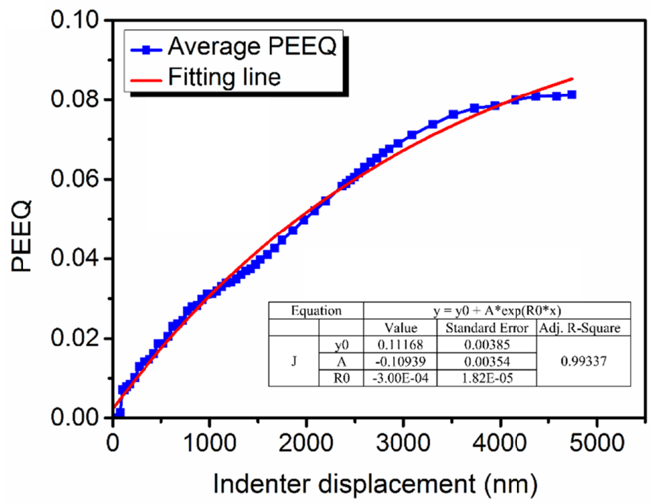

Fig. 11. The fitting results of average PEEQ

Fig. 12 compares the indentation characteristic strain from damage and average PEEQ. Both show the same change trend with increasing the indentation depth, but the average PEEQ has greater values than indentation characteristic strain in the indentation depth range from 0 to 11000 nm. According to Eq. (3) and (6), there is a same parameter h, so it can be induced the relationship between strain and PEEQ. The expression can be written as below:

$$\varepsilon = 0.12703 - 0.25941(0.11168 - PEEQ_{FEM})^{0.3056} \qquad (7)$$

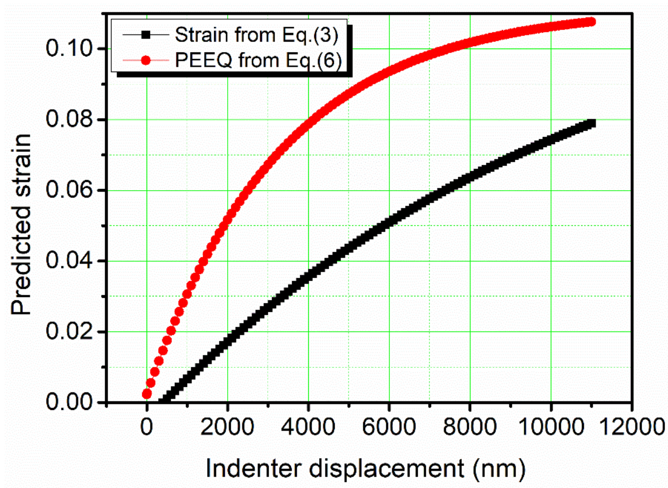

Fig. 12. Predicted strain for different indenter displacement

4. Conclusions

In this work, the indentation characteristic strain was studied on Al 5052 based on damage. The indentation simulation was carried out for strain statistics. Some conclusion can be drawn as follows.

(1) The indentation characteristic strain can be determined from damage. A function of indentation characteristic strain on indentation depth is determined. According to this function, the limitation of indentation characteristic strain is 0.12703. Also, the damage with the indentation depth is rewritten, which has a limitation of 0.85 for Al5052. This indicates that failure would not occur in this material at great indentation depth.

(2) The average PEEQ is calculated from simulation results. The average PEEQ is a function of indentation depth, which increases with increasing the indentation depth. The limitation of average PEEQ is 0.11168, which well agrees with the Tekkaya's result.

(3) Comparison between the indentation characteristic strain from damage and average PEEQ indicates that they show the same changing trend with increasing the indentation depth. The average PEEQ is greater than the indentation characteristic strain when the indentation depth is less than 12 μm. Furthermore, the relationship between the indentation characteristic strain and the average PEEQ have be deduced.

CRediT authorship contribution statement

Hao Zhang: Investigation, Methodology, Visualization. Zhibo Guo: Investigation. Zhanwei Yuan: Resources, Writing-review & editing, Supervision.

Declaration of competing interest

The authors declare that they have no known competing financial interests or personal relationships that could have appeared to influence the work reported in this paper.

REFERENCE

[1] D. Tabor, The hardness of metals, Clarendon Press1951.

[2] N.A. Branch, G. Subhash, N.K. Arakere, M.A. Klecka, Material-dependent representative plastic strain for the prediction of indentation hardness. Acta Materialia **58** (19), 6487-6494 (2010).

[3] Y.-T. Cheng, Z. Li, Hardness obtained from conical indentations with various cone angles. Journal of Materials Research **15** (12) 2830-2835 (2000).

[4] A.G. Atkins, D. Tabor, Plastic Indentation In Metals With Cones **13** (3), 149-164 (1965).

[5] K.L. Johnson, The correlation of indentation experiments. Journal of the Mechanics & Physics of Solids **18** (2) 115-126 (2021).

[6] S. Jayaraman, G. Hahn, W. Oliver, C. Rubin, P. Bastias, Determination of monotonic stress-strain curve of hard materials from ultra-low-load indentation tests. International Journal of Solids and Structures **35** (5), 365-381 (1998).

[7] H. Chen, Z. Fu, D. Chen, H. Peng, W. Li, Z. Meng, Z. Fan, A unified sharp indentation method for obtaining stress-strain relations, strength and Vickers hardness of ductile metallic materials. Materials Today Communications **33**, 104652 (2022).

[8] G. Han, L. Cai, H. Xiao, M. Huang, A novel flat indentation test method for obtaining stress–strain relationships of metallic materials based on energy density equivalence, International Journal of Solids and Structures **269**, 112195 (2023).

[9] M. Dao, N. Chollacoop, K. Van Vliet, T. Venkatesh, S. Suresh, Computational modeling of the forward and reverse problems in instrumented sharp indentation. Acta Materialia **49** (19), 3899-3918 (2001).

[10] N. Ogasawara, N. Chiba, X. Chen, Representative strain of indentation analysis. Journal of Materials Research **20** (8), 2225-2234 (2005).

[11] Y. Li, D. Omacht, F. Yu, M. Sun, A new spherical indentation approach to determine fracture toughness of high strength steels. Engineering Fracture Mechanics **272**, 108695 (2022).

[12] J.D. Clayton, J.T. Lloyd, D.T. Casem, Simulation and dimensional analysis of instrumented dynamic spherical indentation of ductile metals. International Journal of Mechanical Sciences **251**, 108333 (2023).

[13] M. Idriss, O. Bartier, D. Guines, L. Leotoing, G. Mauvoisin, X. Hernot, Instrumented indentation for determining stress and strain levels of pre-strained DC01 sheets. International Journal of Mechanical Sciences **238**, 107833 (2023).

[14] A. Bolshakov, G. Pharr, Influences of pileup on the measurement of mechanical properties by load and depth sensing indentation techniques, Journal of Materials Research **13** (4, 1049-1058 (1998).

[15] J.M. Antunes, J.V. Fernandes, L.F. Menezes, B.M. Chaparro, A new approach for reverse analyses in depth-sensing indentation using numerical simulation. Acta Materialia **55** (1), 69-81 (2006).

[16] Y. Cao, N. Huber, Further investigation on the definition of the representative strain in conical indentation. Journal of Materials Research **21** (07), 1810-1821 (2004).

[17] M.M. Chaudhri, Subsurface strain distribution around Vickers hardness indentations in annealed polycrystalline copper. Acta Materialia **46** (9), 3047-3056 (1998).

[18] Z. Yuan, Y. Wang, W. Tian, Y. Wang, K. Wang, F. Li, Y. Guo, Y. Hu, X. Wang, The relationship between plastic zone and contact radius during indentation experiment for strain-hardened materials. Philosophical Magazine Letters, 209-217 (2017).

[19] J.L. Bucaille, S. Stauss, E. Felder, J. Michler, Determination of plastic properties of metals by instrumented indentation using different sharp indenters. Acta Materialia **51**, 1663-1678 (6).

[20] K. Eswar Prasad, N. Chollacoop, U. Ramamurty, Role of indenter angle on the plastic deformation underneath a sharp indenter and on representative strains: An experimental and numerical study. Acta Materialia **59** (11), 4343-4355 (2011).

[21] J. Dong, F. Li, C. Wang, Micromechanical behavior study of α phase with different morphologies of Ti–6Al–4V alloy by microindentation. Materials Science and Engineering: A **580**, 105-113 (2013).

[22] M. He, F. Li, N. Ali, A normalized damage variable for ductile metals based on toughness performance. Materials Science & Engineering: A **528** (3), 832-837 (2011).

[23] Z. Yuan, C. Wang, F. Li, Y. Hu, Y. Guo, Q. Chen, Y. Wang, M. Guo, Investigation on Behavior of Elastoplastic Deformation for Ti–48Al–2Cr–2Nb Alloy by Micro-Indentation and FEM-Reverse Algorithm. Advanced Engineering Materials **19** (8), 17000971-8 (2017).

[24] Z. Yuan, F. Li, F. Xue, M. Zhang, J. Li, An Investigation of Micro-Mechanical Properties of Al Matrix in SiC/Al Composite by Indentation Experiments. Journal of Materials Engineering and Performance **24** (2), 654-663 (2015).

[25] W.C. Oliver, G.M. Pharr, Measurement of hardness and elastic modulus by instrumented indentation: Advances in understanding and refinements to methodology. Journal of Materials Research **19** (1), 3-20 (2004).

[26] W.C. Oliver, G.M. Pharr, An improved technique for determining hardness and elastic modulus using load and displacement sensing indentation experiments. Journal of Materials Research **7** (6), 1564-1583 (1992).

[27] J. Li, F. Li, F. Xue, J. Cai, B. Chen, Micromechanical behavior study of forged 7050 aluminum alloy by microindentation. Materials & Design **37**, 491-499 (2012).

[28] J. Li, F. Li, M. He, F. Xue, M. Zhang, C. Wang, Indentation technique for estimating the fracture toughness of 7050 aluminum alloy with the Berkovich indenter. Materials & Design **40**, 176-184 (2012).

[29] M. Zhang, F. Li, Z. Yuan, J. Li, S. Wang, Effect of heat treatment on the micro-indentation behavior of powder metallurgy nickel based superalloy FGH96. Materials & Design **49**, 705-715 (2013).

[30] C.C. Tasan, J.P.M. Hoefnagels, M.G.D. Geers, Identification of the continuum damage parameter: An experimental challenge in modeling damage evolution. Acta Mater **60** (8), 3581-3589 (2012).

[31] K. Johnson, The correlation of indentation experiments. Journal of the Mechanics and Physics of Solids **18** (2), 115-126 (1970).

[32] A.E. Tekkaya, K. Lange, An Improved Relationship between Vickers Hardness and Yield Stress for Cold Formed Materials and its Experimental Verification. CIRP Annals – Manufacturing Technology **49** (1), 205-208 (2000).

[33] V.V. Bulatov, W.G. Wolfer, M. Kumar, Shear impossibility: Comments on "Void growth by dislocation emission" and "Void growth in metals: Atomistic calculations". Scripta Mater **63** (1), 144-147 (2010).

[34] G. Monnet, Mechanical and energetical analysis of molecular dynamics simulations of dislocation–defect interactions. Acta Materialia **55** (15), 5081-5088 (2007).

[35] M. Zhang, F. Li, Z. Yuan, J. Li, S. Wang, Effect of heat treatment on the micro-indentation behavior of powder metallurgy nickel based superalloy FGH96. Materials & Design **49**, 705-715 (2013).

[36] R. Billardon, L. Moret-Bailly, Fully coupled strain and damage finite element analysis of ductile fracture. Nuclear Engineering & Design **105** (1), 43-49 (1987).

[37] J.S. Cope, D. Corney, J.Y. Clark, P. Remagnino, P. Wilkin, Plant species identification using digital morphometrics: A review. Expert Systems with Applications (39), 7562-7573 (2012).

[38] Z. Yuan, Y. Wang, W. Tian, Y. Wang, K. Wang, F. Li, Y. Guo, Y. Hu, X. Wang, The relationship between plastic zone and contact radius during indentation experiment for strain-hardened materials. Philosophical Magazine Letters **98** (5), 209-217 (2018).

[39] K. Durst, B. Backes, O. Franke, M. Göken, Indentation size effect in metallic materials: Modeling strength from pop-in to macroscopic hardness using geometrically necessary dislocations. Acta Materialia **54** (9), 2547-2555 (2006).

[40] Q. Ma, D.R. Clarke, Size dependent hardness of silver single crystals. Journal of Materials Research **10**, 853-863 (1995).